Evolution of inverse cascades and formation of precondensate in Gross-Pitaevskii turbulence in two dimensions

Natalia Vladimirova
Department of Mathematics and Statistics, University of New Mexico, Albuquerque, New Mexico 87131, USA
(Received 19 September 2017; published 13 December 2017)

Here we study how coherence appears in a system driven by noise at small scales. In the wave turbulence modeled by the Gross-Pitaevskii or the nonlinear Schrödinger equation, we observe states with correlation scales smaller than the system size but much larger than the excitation scale. We call a such state precondensate to distinguish it from condensate defined as a systemwide coherent state. Both condensate and precondensate are characterized by large-scale phase coherence and a narrow distribution of amplitudes. When one excites small scales, precondensate is achieved relatively quickly by an inverse cascade heating quasiequilibrium distribution of large-scale modes. The transition from the precondensate to the systemwide condensate requires a much longer time. The spectra of precondensate differ from quasiequilibrium and are characterized by two bending points, one on the scale of the average distance between vortex pairs and the other on the scale of the distance between vortices in a pair. We suggest temporal evolution laws for both lengths and use them to predict the probability of the transition to condensate.

DOI: 10.1103/PhysRevE.96.062206

In nonlinear systems, a conserved quantity can be distributed among a large number of degrees of freedom. Such systems are commonly studied in spectral space where the nonlinear interaction of modes becomes more apparent. If the conserved quantity is deposited in a narrow range of modes, or on a particulate length scale, larger and smaller scales eventually become excited. The most notable examples are the redistribution of energy between scales of fluid turbulence and the redistribution of wave action in wave turbulence. The presence of a second conserved quantity (enstrophy in two-dimensional fluid turbulence or energy in wave turbulence) additionally requires transfer to large scales in the so-called inverse cascade. Unless infinite space is considered, the inverse cascade is restricted by the size of the system. The persistent excitation of small scales can lead to accumulation of the conserved quantity on the scale of the system, the turbulent formation of condensate. In two-dimensional fluid turbulence the condensate appears as a systemwide vortex; in wave turbulence the condensate is a background state with a fast-rotating phase and uniform intensity.

When the separation of scales is large, the condensate can be difficult to build up. There is no general recipe on how long and how strongly one needs to pump the system to observe the condensate. The shape of the evolving spectrum is also not known. In the weak wave turbulence theory [1], which assumes an interaction local in k space and reduces the description to a kinetic wave equation, frontlike spectra were observed for inverse and direct cascades in hydrodynamic turbulence [2] and for direct cascades in more general settings [3]. In the models that account for phase interactions of modes, such as the Gross-Pitaevskii (GP) model [4], the spectra can spread out rapidly with nontrivial shapes, as was shown in [5,6]. This suggests the importance of nonlocal interactions in the GP system.

The Gross-Pitaevskii equation, also known as the nonlinear Schrödinger equation, is one of the most studied in modern physics because of its universality. The equation is applicable to a wide range of phenomena in fluids, solids, and plasma, including nonequilibrium states of cold atoms in Bose-Einstein condensates [4] and propagation of light in media with the Kerr nonlinearity [7]. In two dimensions, the equation describes the evolution of a complex wave envelope ψ,

$$\psi_t = i\nabla^2\psi + is|\psi|^2\psi, \tag{1}$$

with wave action $N = \langle|\psi|^2\rangle$ being the conserved quantity in question. Here s distinguishes focusing (attractive) ($s = +1$) and defocusing (repulsive) ($s = -1$) nonlinearity and the angular brackets denote averaging in space.

When applied to the GP equation, weakly nonlinear theory predicts the formation of large structures for both focusing and defocusing nonlinearities [1]. However, with an increase of nonlinearity, these large structures become unstable if nonlinearity is focusing [8]. This suggests that the condensate can be observed only in the defocusing case [5,9]. Accumulation of wave action in defocusing systems leads to a different kind of coherent structure, vortices, i.e., locations with zero amplitude, around which the phase makes a 2π turn. As shown in Refs. [6,10,11], a decrease in number of vortices leads to the formation of condensate.

In this paper we study the evolution of turbulence in the GP model during persistent excitation of small scales. Our goals are to (i) explore the possibility of the appearance of local order on scales smaller than the domain size, (ii) establish a connection between time-dependent spectra and the phase coherence of the system, in particular the evolution of vortices, and (iii) study the effect of system size on its evolution and make a qualitative prediction of the probability of formation of systemwide condensate in domains of finite size.

We stress that the key focus of this study is turbulence evolution. Our earlier work [12] was devoted to the fluxes of direct and inverse cascades in a steady state of the GP system stabilized by large-scale friction. While we have observed some midrange distortion of the spectra, which was independent of the domain size and similar to the that described below, the large-scale modes were suppressed by friction. It is those modes that influence the midrange modes via nonlocal interactions, making the distortion the feature

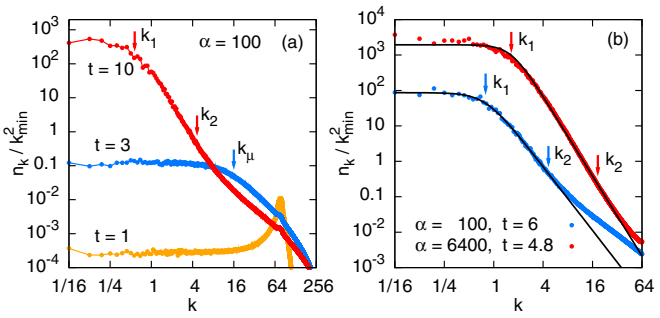

FIG. 1. (a) Typical spectra of wave action at very early, early, and late stages of evolution. (b) Spectra at late times fitted by Eq. (4). Here k_μ marks the bending point in early spectra, while k_1 and k_2 are bending points in late spectra; $k_{\min} = 2\pi/L$, where L is the size of the system.

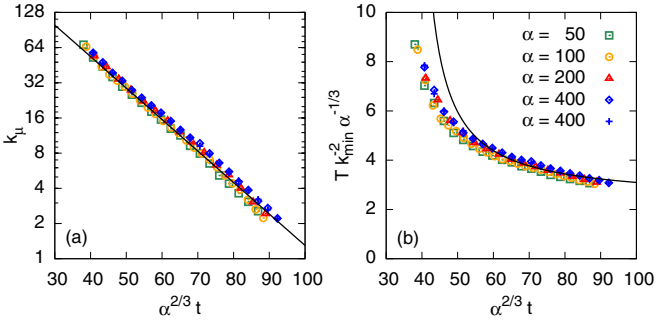

FIG. 2. Chemical potential and temperature at early times for different α. All points, except crosses, are data from simulations with $L = 8\pi$; crosses are data from simulations with $L = 32\pi$. The lines show the dependence $k_\mu = C\exp(-c\alpha^{2/3}t)$ and T given by Eq. (3) with $C = 640$ and $c = 0.062$.

of steady spectra, in the way that the obtained flux law was specific to the steady system. Naturally, a steady setup cannot inform one on the time scale of the establishment of the condensate, while here we propose a quantitative estimate of the time of formation of the condensate under a constant pumping rate.

Similarly to [12], we numerically solve Eq. (1) with focusing nonlinearity as described in Appendix A. The wave action is deposited at the rate α in a ring of wave numbers at $k \approx k_p$ and accumulates in the system at the rate $\tilde{\alpha} \approx 0.92\alpha$. Initially, the spectrum of the wave action is empty, $n_k \equiv |\psi_k|^2 = 0$. The first excited modes appear in the pumping ring. Our intuition might tell us that modes with close $\mathbf{k}$ interact more effectively, resulting in a gradual widening of the spectrum beyond the pumping ring. Apparently this is not the case. Already after the time period comparable to the nonlinear interaction time, we observe a uniform distribution of n_k for $k < k_p$, as well as for $k > k_p$. The spectrum at $k < k_p$ remains flat, with n_k growing in time; the spectrum at $k > k_p$ is more complex as it is affected by damping. We observe the scaling $n_k \propto \alpha$ for the forced modes and scaling $n_k \propto \alpha^3$ for the nonforced modes. The second scaling follows from the first one and from cubic nonlinearity. The flat shape of n_k most likely is the consequence of a circular arrangement of forced modes. The simultaneous growth of all modes illustrates the importance of nonlocal interactions already at the beginning of evolution. Indeed, the plateau that extends from $k = 0$ to the forcing ring is a characteristic of very early spectra, as can be seen in Fig. 1.

With time, the peak at the forcing becomes smaller, the height of plateau rises, and a section of sloped spectrum develops between the plateau and the forced modes. This shape of the spectrum can be described by the time-dependent energy-action equipartition

$$n_k = \frac{T(t)}{k_\mu^2(t) + k^2}, \tag{2}$$

where T and $\mu \equiv k_\mu^2$ can be interpreted as the temperature and chemical potential, respectively. The temperature controls the height of the sloped part of the spectra, $n_k \approx T/k^2$, while k_μ corresponds to the bending point at the end of the plateau.

Both T and k_μ decrease with time, as shown in Fig. 2. The fit by Eq. (2) can be applied to the data only when $k_\mu < k_p$, yet the very early rise of the flat spectrum can be seen as the same process. Initially, the chemical potential is so large that $k_\mu(t) > k_p$ and most of the waves at $k < k_p$ appear in the state of action equipartition. Filling the system with waves, we decrease the chemical potential; after k_μ decreases below k_p we start seeing the part of energy equipartition $n_k \propto k^{-2}$ simultaneously with the rise of the plateau.

As shown in Fig. 2, the data from simulations at different pumping rates α and in domains of different sizes collapse onto a single curve when rescaled with α. The decay of k_μ is exponential, while T approaches an asymptote. The exponential decay of k_μ follows from the linear growth of the wave action $\int n_k d\mathbf{k} \approx T\ln(k_p/k_\mu) \simeq \tilde{\alpha}t$, under the assumption that the temperature must eventually saturate. Then, assuming the dependence $k_\mu = C\exp(-c\alpha^{2/3}t)$, suggested by data, one can find the temperature in the limit of $k_\mu \ll k_p$,

$$\frac{T}{k_{\min}^2} = (2\pi)^{-1}\frac{\tilde{\alpha}t - N_p}{c\alpha^{2/3}t - \ln(A/k_p)}, \tag{3}$$

where $k_{\min} = 2\pi/L$ in a system of size L and N_p is the number of waves at $k > k_p$; in our simulations $N_p \approx c^{-1}\alpha^{1/3}$. The dependence explains the collapse of data in coordinates $(\alpha^{2/3}t, T\alpha^{-1/3})$ observed in Fig. 2.

The scaling of temperature with α is consistent with weakly nonlinear theory. We expect that, if the nonlinearity is weak, the flux is cubic in wave numbers n_k [1] so that $T \propto \alpha^{1/3}$ and $\ln k_\mu \propto \alpha^{2/3}t$, which is indeed seen in Fig. 2. In general, the scaling for temperature and conservation of wave action lead to the scaling of time with α,

$$\dot{N} \sim \dot{T} \sim \alpha \Rightarrow T/t \sim \alpha \Rightarrow t \sim \alpha^{1/3}\alpha^{-1} \sim \alpha^{-2/3}.$$

One might find the decrease of the temperature with time counterintuitive. We think it can be interpreted again in terms of a nonlocal interaction: To carry the same flux through a longer spectrum one needs smaller amplitude. In other words, the nonlocal transfer of wave action through a given k is determined by both the amplitude and the extent of the interval. When the interval expands towards lower k and acquires higher n_k at low k, the transfer becomes more effective and the magnitude decreases.

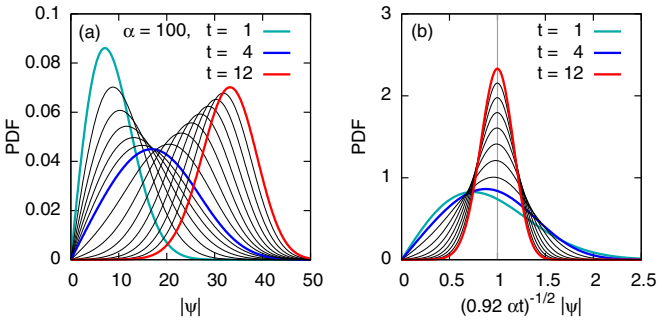

FIG. 3. The PDF of $|\psi|$ in (a) simulation units and (b) units rescaled with $N = \tilde{\alpha}t = 0.92\alpha t$.

As time passes and wave action accumulates, the system transitions to a different regime where the spectra have two bending points and the fit by Eq. (2) no longer applies (see Fig. 1). A similar transition occurs in systems with focusing nonlinearity, as shown in Appendix B. The transition time $t^* \approx 90\alpha^{-2/3}$ and corresponding $k_\mu \approx 2$ are surprisingly universal. Moreover, as we show below, the scaling $\alpha^{2/3}t$ well describes evolution in the new nonlinear regime, even though this scaling was obtained under the assumption of weak nonlinearity. This is somewhat surprising.

Even more dramatically than in spectra, the transition to the new regime is seen in the probability density function for $|\psi|$, shown in Fig. 3. Here we follow the evolution of the distribution of amplitudes with respect to the time-dependent average $\chi = |\psi|/|\psi|_{\rm rms} = N^{-1/2}|\psi|$. At the early stage, the distributions of real and imaginary parts of ψ are Gaussian with zero average, so the distribution of the magnitude has the form $\mathcal{P}(\chi) = 2\chi e^{-\chi^2}$; at this stage the standard deviation for $|\psi|$ widens with time, $\sigma = \frac{1}{2}N^{1/2}$.

In contrast, in the new regime the distribution narrows and shifts toward higher amplitudes. The maximum is located at $|\psi| = N^{1/2}$, while the overall shape closely resembles a Gaussian distribution, $\ln \mathcal{P}(|\psi|) \propto -(|\psi| - N^{1/2})^2/\sigma^2(t)$. The probability of small fluctuations $|\psi| \ll N^{1/2}$ is determined by vortices (see Appendix C for more details). Figure 4 shows the growth of $\langle|\psi|\rangle$, which scales as $t^{1/2}$ during both early and later stages; it also shows a nonmonotonic time dependence for σ. The time when the distribution is the widest is easily detectable, $t^* \approx 90\alpha^{-2/3}$. We use this time

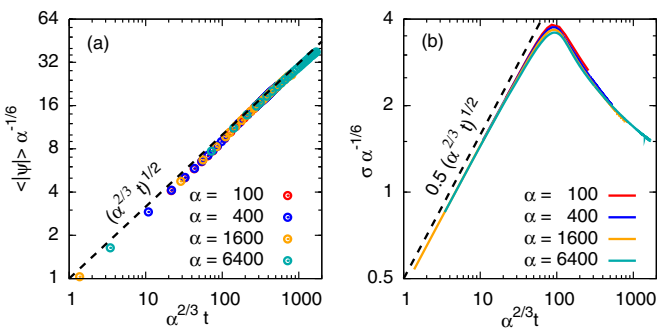

FIG. 4. (a) Average and (b) standard deviation for distribution of $|\psi|$ as a function of time, in units scaled with α.

as the definition for the transition between the earlier and later regimes.

The narrow distribution of $|\psi|$ is a prominent feature of systemwide condensates, where most of the wave action resides in the single mode, $k = 0$, while other waves add a small distortion to the condensate's background. In the case considered here, the background is formed by multiple modes, so we refer to the state at $t > t^*$ as precondensate, as opposed to systemwide condensate.

Another feature of condensates is the phase coherence. In a system with a systemwide condensate there are no vortices and the phase across the domain only slightly deviates from the phase of the zeroth mode. Precondensate at its later stages can have most of the wave action absorbed in the $k = 0$ mode yet only partial phase coherence because of the presence of vortices. In such cases the scale of phase coherence is the typical distance between vortices [6,10,11].

Our simulations show that t^* corresponds to the time when distinct vortices start to appear. At $t < t^*$ the probability of a near-zero $|\psi|$ is high, the phase correlation length is short, and formal detection of vortices returns vortex locations all over the computational grid. If the vortex is a "hole" in the background amplitude, to have vortices we need to have a nonzero background. At $t \approx t^*$ such a background begins to form.

During the time interval $t^* \lesssim t \lesssim 2t^*$ the distance between detected vortices is still of the order of grid resolution, but the number of vortices drops sharply. At $t \gtrsim 2t^*$, the vortices can be located by visual inspection of the phase field; their number decreases in time, but much slower. One can think of the state at $t < t^*$ as containing no distinct vortices, the time interval $t^* < t < 2t^*$ as the stage of vortex formation, and $t > 2t^*$ as the stage of vortex annihilation.

Figure 5 shows snapshots of the phase for two pumping rates at two times. Notice that the system with $\alpha = 6400$ and $t = 4.7$ has a smoother phase than the one with $\alpha = 100$ and $t = 8$; this is because the transition time scale is shorter for stronger pumping, $t^* = 0.26$ versus $t^* = 4.2$. Also notice that vortices form pairs and that the typical distance between vortices in a pair remains constant over the course of evolution, while the number of pairs decreases. Finally notice that the system with higher pumping rate has more vortex pairs and a shorter distance between vortices in a typical pair.

To quantify these observations, we have implemented diagnostics of vortices and vortex pairs, described in Appendix C. If we denote the number of vortices of the same sign (half the total number of vortices) by $n_{\rm vort}$, then the typical distance between isolated vortices or vortex pairs is $d_1 = Ln_{\rm vort}^{-1/2}$. The typical distance between vortices in a pair, d_2, is estimated from the distribution of distances $d_2^{(i)}$ of individual pairs.

We found that the number of vortices scales with $\alpha^{2/3}t$ and decreases with time. The time range is too short to suggest a functional dependence; while both a power law and a logarithmic dependence are possible, for the interpolation purposed we adopted the power law. The length of a vortex pair depends on the pumping rate, rather than time, which is surprising and deserves further investigation, as discussed in Appendix C.

Next we connect the statistics of vortices to the evolution of spectra $n_k(t)$. In the precondensate regime $t > t^*$, the spectra have two bending points k_1 and k_2, as shown in Fig. 1. An

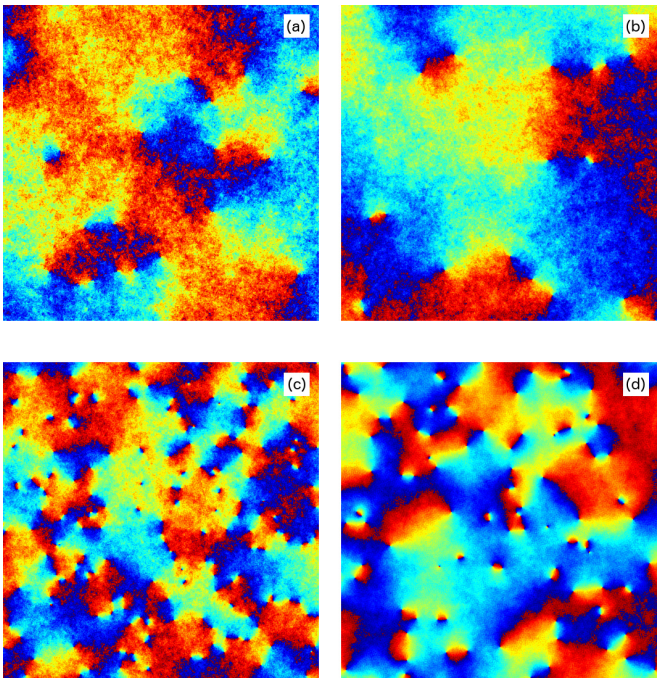

FIG. 5. Phase in a fraction of the domain $L/8 \times L/8$, from simulations with $L = 32\pi$, for (a) $\alpha = 100$ and $t = 8$, (b) $\alpha = 100$ and $t = 12$, (c) $\alpha = 6400$ and $t = 0.1$, and (d) $\alpha = 6400$ and $t = 4.7$. The images illustrate that the typical distance between vortex pairs d_1 increases in time, the typical scale of the vortex pair d_2 remains constant, and the distance between the vortices in a pair d_2 is smaller for larger α.

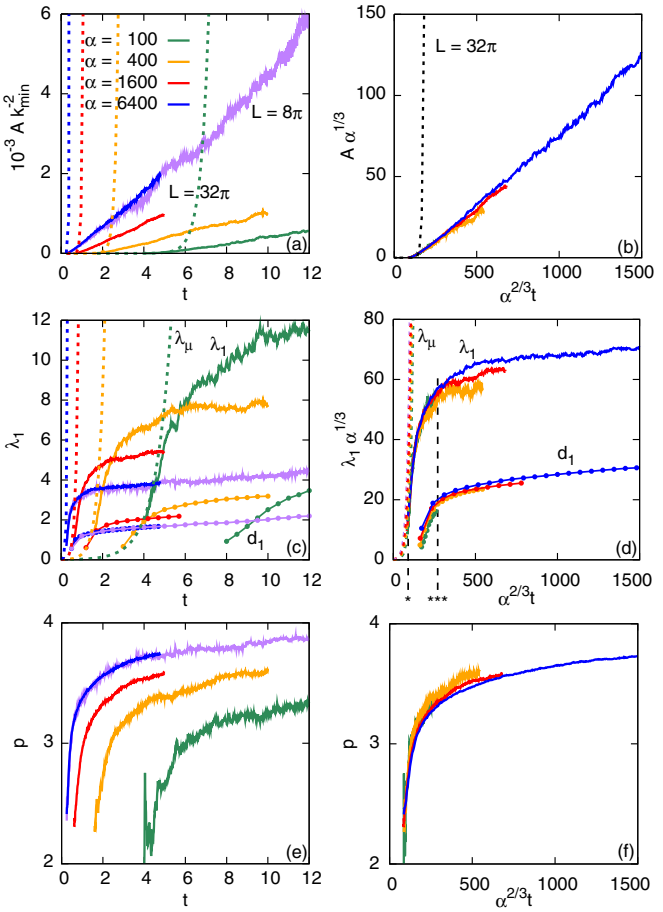

FIG. 6. Parameters in late evolution spectra, A, $\lambda_1 = 2\pi/k_1$, and p, as a function of time in simulation and rescaled units. The purple line corresponds to $\alpha = 6400$ and $L = 8\pi$; all other data are from $L = 32\pi$ simulations. Dotted lines show the extrapolations from the weakly nonlinear regime, with $A = T/k_\mu^2$ and $\lambda_\mu = 2\pi/k_\mu$. In (c) and (d) the typical distance between vortices $d_1 = Ln_{\text{vort}}^{-1/2}$ is shown with connected points; dashed vertical lines indicate the times t^* and $3t^*$.

equipartition shelf at small k meets a slope steeper than k^{-2} at $k = k_1$; this slope transitions to a slope close to k^{-2} at $k = k_2$. We fit the spectra in the range $[k_{\min}, k_2]$ using the function

$$n_k = \frac{A}{1 + (k/k_1)^p}. \tag{4}$$

Here p is some power and A is the height of the equipartition shelf. When $p = 2$, $k_1 = k_\mu$, and $A = T/k_\mu^2$, the fit reduces to Eq. (2).

Figure 6 shows how the parameters of the spectra in Eq. (4) change with time. After the transition, the height of the shelf rises linearly with time, as $A \propto \alpha^{1/3} t$, in contrast to early evolution, when the height of the shelf T/k_μ^2 grows exponentially (due to exponential decay of k_μ). The scale associated with the first bending point in the spectra, $\lambda_1 = 2\pi/k_1$, initially grows rapidly, yet not as fast as exponentially increasing $\lambda_\mu = 2\pi/k_\mu$. At the time $t \sim 3t^*$ the growth of λ_1 slows down. The scale λ_1 appears to be proportional to the distance between vortex pairs, $\lambda_1 \sim 2.5 d_1$, so we conclude that the first bending point in the spectra marks the scale of phase coherence or the scale of patches of precondensate. The third parameter, power p, describes the slope of the spectrum after the plateau, in the $k_1 < k < k_2$ range. This slope steepens with time from $p = 2$ in the thermal equilibrium regime to possibly $p = 4$ in the long-running evolution.

If k_1 corresponds to the distance between vortex pairs d_1, the natural question arises: What scale corresponds to k_2? We notice that the second bending point of the spectrum does not move over the course of evolution; however, it shifts to the smaller scales as α increases. Recall that we made the same observation about the typical distance between vortices in a pair, d_2. Indeed, the corresponding wave number $k_2 = \alpha^{1/3}$ is located approximately at the second bending point of the spectra (see Appendix C for details). Thus, the data suggest that $\lambda_2 = d_2 = 2\pi\alpha^{-1/3}$ is the typical distance between vortices in a vortex pair.

The emergence of a second inflection point and deviation from thermal equilibrium spectra can be interpreted as an internal bottleneck effect. The pileup occurs at wave numbers where the nonlinearity is getting substantial. We have observed a similar pileup in simulations stabilized by low-k friction [12], where, regardless of the domain size, stronger nonlinearity leads to more pileup, while pumping at lower rate reduces piling up and extends the universal part of the spectrum.

Until now we have studied the evolution of wave turbulence before it gets affected by the size of the domain. Now we are interested in the transition from precondensate to a systemwide

condensate. We need relatively long simulations in relatively small boxes, so we can watch all vortices disappear. We expect this to happen when the typical distance between vortices d_1 exceeds the domain size.

We found that the number of vortices in domains with sizes $L = 2\pi$, π, and $\pi/2$ follows the same dynamics as our large-scale simulations, $L = 32\pi$, provided that the evolution in small boxes is interpreted in the statistical sense. (We have considered ensembles of multiple realizations for each combination of parameters; see Appendix D for details.) The chance of a transition to condensate is much higher when d_1 exceeds the domain size during the vortex formation stage; during the vortex annihilation stage precondensate slows down the annihilation of vortices. For the creation of systemwide condensate, slow pumping rates are favorable, since d_1 is an increasing function of $\alpha^{2/3}t$. In general, one can predict the typical time of transition to condensate by solving $d_1(\alpha^{2/3}t) = L$. This statement is not obvious, since one could expect the limited size of the system to have an additional effect.

Once the condensate has been established, the spectra for over-condensate fluctuations are expected to have slope $n_k \propto k^{-2}$ [5,13]. Unfortunately, we could not detect the transition from the k^{-p} spectrum for a precondensate to the k^{-2} spectrum of over-condensate fluctuations. This is because, to resolve precondensate spectra, we need many modes and large domains, while slow annihilation of vortices requires long simulation times. All simulations where we could achieve a transition to systemwide condensate are done in small boxes. In these simulations, the spectra never have a chance to develop slopes with $p > 2$. Instead, they transition from the thermal equilibrium spectrum with $p = 2$ directly to the spectrum with $p = 2$ for over-condensate fluctuations.

In this work we have used the model of the Gross-Pitaevskii or the nonlinear Schrödinger equation to study the evolution of wave turbulence excited by small-scale forcing. While the wave action accumulates in a system at a constant rate, there is a time t^* that marks the transition from a weakly nonlinear to a substantially nonlinear regime (when the focusing case and the defocusing case start to deviate, as shown in Appendix B). At $t < t^*$ the spectra of n_k have the form of a time-dependent energy-action equipartition, while the distribution of $|\psi|$ widens with time. At $t > t^*$ the distribution of $|\psi|$ in the defocusing case is concentrated near the rising background (precondensate), while spatial locations with near-zero $|\psi|$ become sparse and develop a vortex structure. The typical distance between vortex pairs and the typical distance between vortices in a pair correspond to two bending points in the spectra of the wave action.

The evolution of vortex density in a large domain well describes the probability of developing a systemwide condensate in a small domain. The condensate is more likely to appear if the number of vortex pairs is expected to drop below 1 during the vortex generation stage, $t^* \lesssim t \lesssim 3t^*$. Later, at $t \gtrsim 3t^*$, strong precondensate prevents vortex interaction and vortex annihilation slows down. The rescaling between nondimensional units and physical units and the estimate for the transition time t^* in physical units are shown in Appendix E.

I thank G. Falkovich for encouragement, discussions, and reading a draft of the paper. The work was supported by NSF Grant No. DMS-1412140. Simulations were performed at Texas Advanced Computing Center using Extreme Science and Engineering Discovery Environment, supported by NSF Grant No. ACI-1548562 through allocation TG-DMS140028.

APPENDIX A: NUMERICAL SETUP

Our setup is almost identical to that in [12], where we studied the inverse cascade stabilized by large-scale friction, with the exception that now the friction is turned off. The wave action is deposited at the rate α in a ring of wave numbers $k \in [k_l, k_r]$. Some fraction of it is lost to small-scale damping, applied at $k > k_d \approx 3k_r$; the rest accumulates in the system at the rate $\dot{N} = \tilde{\alpha}$. The forcing and damping are represented on the right-hand side of the equation,

$$i\psi_t + \nabla^2\psi + s|\psi|^2\psi = i\hat{f}_k\psi + i\hat{g}_k. \tag{A1}$$

Forcing and damping are both applied in spectral space. The forcing is additive, $g_k = |g_k|e^{i\phi_k}$, with random phases ϕ_k and amplitudes $|g_k| \propto \sqrt{(k^2 - k_l^2)(k_r^2 - k^2)}$, while the damping is multiplicative, $f_k = -\beta(k/k_d)^4(k/k_d - 1)^2$. Equation (A1) is solved using a standard split-step method [5] modified to be fourth-order accurate in time.

Our computational domains are square, $L \times L$, with periodic boundary conditions, so the lowest wave number is determined by the domain size, $k_{\min} = 2\pi/L$. The highest wave number is the same in all simulations, $k_{\max} = \pi/\Delta x = 512$, as well as the parameters $k_l = 68$, $k_r = 84$, $k_d = 256$, and $\beta = 400$. This choice of parameters gives 8% loss of wave action in most of simulations, $\tilde{\alpha} = 0.92\alpha$. We model systems with different strengths of forcing, $\alpha = 100$, 400, 1600, and 6400, and of different sizes, up to $L = 32\pi$. Note that our main results are scaled with α and $k_{\min}$, so the forcing length scale is the only fixed parameter in our study. This restriction can be relaxed by rescaling of units described in Appendix E.

As a remark on the size of the simulation we emphasize that the major results reported in this paper, the pileup of wave action at low k and the formation of spectra with two bending points, are not effected by a finite domain size. Most results were obtained in domains with $L = 32\pi$, yet when we repeated some of the simulations in domains $L = 8\pi$, we observed essentially the same behavior (see, for example, the curves for $\alpha = 6400$ in Fig. 6). The largest of the discussed length scales is $\lambda_1 \sim 10$ (at the end of the run with $\alpha = 100$), which is still small compared to $L = 32\pi \approx 100$. The smallest number of vortex pairs used in vortex statistics is 840, also at the end of the run with $\alpha = 100$; this number is large enough to ignore the effects of domain size.

APPENDIX B: FOCUSING CASE

Weakly nonlinear theory does not distinguish positive and negative nonlinearity. So, at very early times, the spectra with focusing and defocusing nonlinearities are expected to evolve in the same way. It turns out that this similarity lasts almost to the end of the weakly nonlinear regime, $t \lesssim t^*$. Figure 7 shows the spectra of focusing and defocusing systems for $\alpha = 100$ ($t^* \approx 4.2$) and for $\alpha = 6400$ ($t^* \approx 0.26$). At the very early

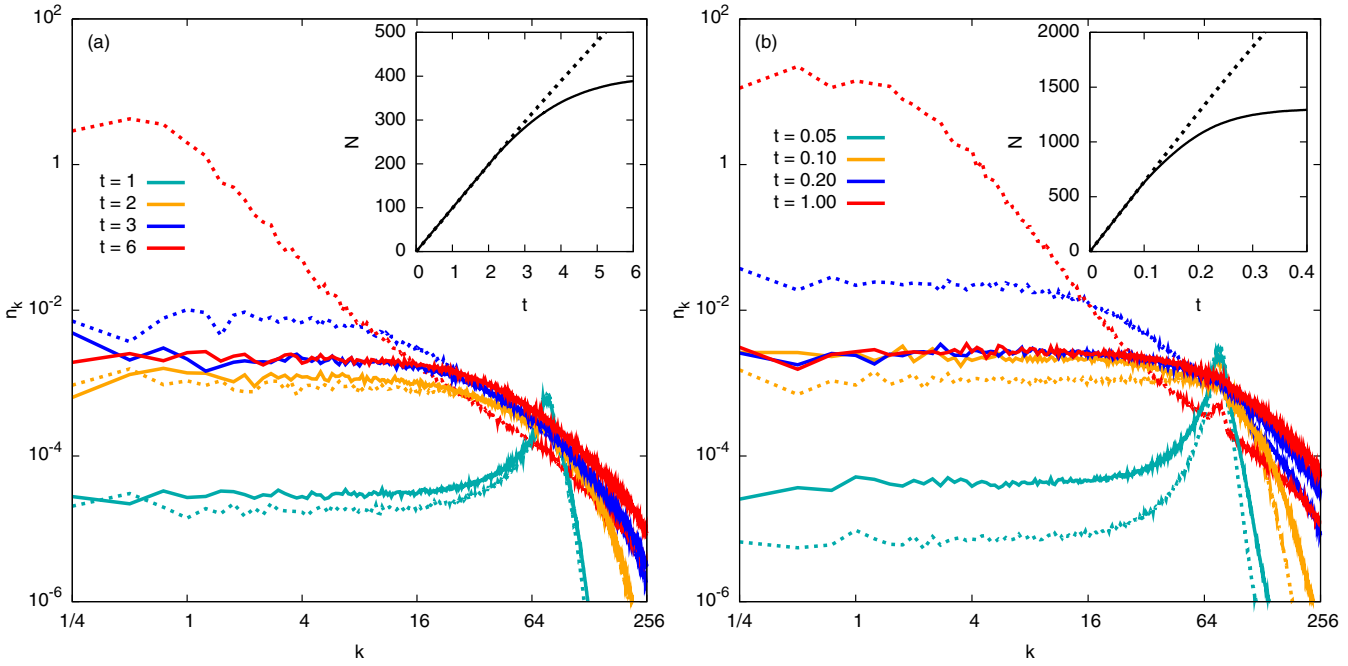

FIG. 7. Comparison of focusing spectra (solid lines) and defocusing spectra (dashed lines) at different times of system evolution for (a) $\alpha = 100$ and (b) $\alpha = 6400$. The insets show the total number of waves.

times, the spectra look qualitatively the same, except that the focusing nonlinearity is more effective in populating low-k modes, especially at higher α, possibly because of a nonlinear shift of frequency and a higher effective nonlinearity parameter $(k^2 \pm N)/k^2$. Since in the weak turbulence approximation the evolution of focusing and defocusing systems must be exactly the same, this small difference in the spectra is already an effect of nonlinearity.

Approximately at the time when defocusing spectra start to deviate from the thermal equilibrium form, focusing spectra stabilize at an equilibrium. This is also seen in the total number of waves (insets in Fig. 7). The stabilization of $N(t)$ at constant pumping is the sign of enhanced loss of wave action due to collapses. Indeed, at $t \approx t^*$ both systems start to develop coherent patches of precondensate. In the focusing case, coherent patches turn into collapses; this process transfers the wave action to high k, where it gets consumed by damping. The stable level of the wave action can be estimated as $N^* \approx \alpha t^* \propto \alpha^{1/3}$. By the order of magnitude that this is seen in simulations, however, the functional dependence appears to be more complex.

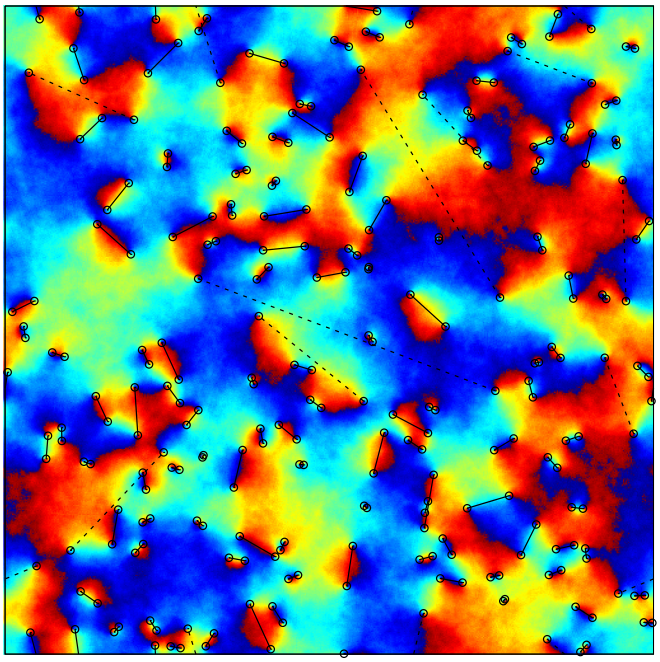

FIG. 8. Diagnostics of vortex pairs. The image shows the phase in the system with $\alpha = 6400$ and $L = 8\pi$ at $t = 12$. The pairs with distance between vortices exceeding $2d_1$, where d_1 is the typical distance between vortex pairs, are marked with dashed lines.

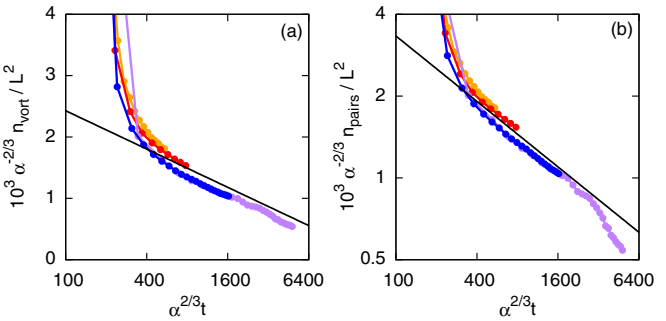

FIG. 9. Number of vortex pairs in (a) lin-log and (b) log-log coordinates obtained in simulations shown in Fig. 6, with line colors matching. The longest range is for $\alpha = 6400$ in the $L = 32\pi$ box (blue) and the $L = 8\pi$ box (purple). The straight lines correspond to $f(t) = 0.0045[1 - 0.1\ln(\alpha^{2/3}t)]$ and to $f(t) = 0.021(\alpha^{2/3}t)^{-2/5}$, respectively.

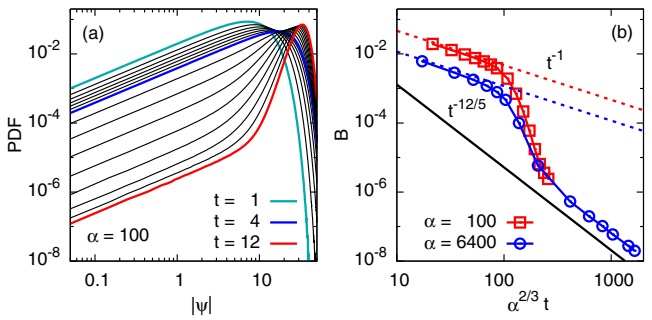

FIG. 10. (a) The probability of small $|\psi|$ is a linear function $\mathcal{P}(|\psi|) = B(t)|\psi|$. (b) The coefficient $B(t)$ drops at the time of transition. At early times, $B = (\tilde{\alpha}t)^{-1}$, shown with dashed lines. At later times, $B(t)$ is proportional to the vortex density: For the number of vortices given by Eq. (C1), it scales as $B \propto (\alpha^{2/3}t)^{-12/5}$.

The last observation suggests that it might be possible to build condensate in a focusing system, if the size of the domain is so small that condensate is formed before the total number of waves reaches a critical wave action, $N_{cr} = 11.7/L^2$. In our setup, however, this would require long simulation times at small pumping rates, $\alpha \propto N^3 \propto L^{-6}$ and $t \sim N\alpha^{-1} \sim L^4$.

APPENDIX C: EVOLUTION OF VORTICES IN RELATION TO THE PROBABILITY OF SMALL AMPLITUDES AND TO SPECTRA

To find the location of vortices we use a method based on the vortex definition. Starting with the phase on a computational grid, ϕ_i^j, we compute the circulation of phase along the perimeter of each computational cell,

$$\delta\phi = \left[\phi_{i+1}^j - \phi_i^j\right] + \left[\phi_{i+1}^{j+1} - \phi_{i+1}^j\right] + \left[\phi_i^{j+1} - \phi_{i+1}^{j+1}\right] + \left[\phi_i^j - \phi_i^{j+1}\right].$$

We restrict each expression in square brackets not to exceed π in absolute value, by adding or subtracting 2π as necessary. The cells with nonzero $\delta\phi$ are recorded as vortices. (We have observed only vortices with a single charge, $\delta\phi = \pm 2\pi$.)

To find vortex pairs, we compute the matrix of distances between positive and negative vortices. Two vortices with the shortest distance are assigned into a pair and excluded from the list. Then the pair with the shortest distance is found again from the reduced matrix and the process is repeated until all vortices are assigned into pairs. This might not be an optimal algorithm, say, in comparison with minimizing the sum of distances over all possible pair assignments, but it is easy to implement and fast to execute. A side effect of this algorithm is a small number of distant vortices formally assigned into pairs; this happens at the end of the assignment procedure because of the lack of unassigned neighbors. Such pairs can be taken out of consideration, if, for instance, their distance exceeds the typical distance between pairs. The results of vortex and vortex pair detection is illustrated in Fig. 8, for a small domain containing 131 vortex pairs. Most of our production runs contain ∼10 000 pairs at the beginning of vortex diagnostics. Subsequently, we implemented even simpler diagnostics, where the length of a pair was computed as the distance to the closest vortex of the opposite sign, and obtained qualitatively the same results.

The number of vortices $n_{\rm vort}$ scales with α and decreases with time, as shown in Fig. 9. The time range is too short to distinguish a power law from a logarithmic dependence, so we restrain from making a statement on the scaling of the number of vortices with time. Yet we need the $n_{\rm vort}(t)$ dependence to estimate the probability of small $|\psi|$ and for comparison with the evolution of small systems. For this purpose, we use the power-law dependence

$$n_{\rm vort} = 0.021 L^2 \alpha^{2/5} t^{-2/5}. \tag{C1}$$

The proposed scaling explains how the probability of small $|\psi|$ decreases with time. Initially, the probability of small amplitudes is $2\chi d\chi = 2N^{-1}|\psi|d|\psi|$, so $\mathcal{P}(|\psi|) \approx B(t)|\psi|$ with $B(t) = 2N^{-1} = 2(\tilde{\alpha}t)^{-1}$. At later times the probability of small amplitudes is determined by the density of vortices and by the profile of an individual vortex. Assuming a radially symmetric vortex, one obtains $|\psi| \sim r$ at the core. If the healing length scales as $N^{-1/2}$ [14], then $|\psi| \sim Nr$. This leads to $B = 4\pi n_{\rm vort}/L^2N^2$, shown in Fig. 10, for $n_{\rm vort}$ given by Eq. (C1). This estimate gives $B \sim (\alpha^{2/3}t)^{-12/5}$ up to a numerical coefficient.

Both logarithmic and power-law scalings for the number of vortices were reported in the literature. Power laws with exponents 0.3–0.4 were observed in relaxation studies [11], with transitional logarithmic scalings. Nazarenko and Onorato [6] reported a logarithmic scaling for forced simulations, but the behavior appears to be transitional as well. It was observed at the early stages, before the formation of precondensate,

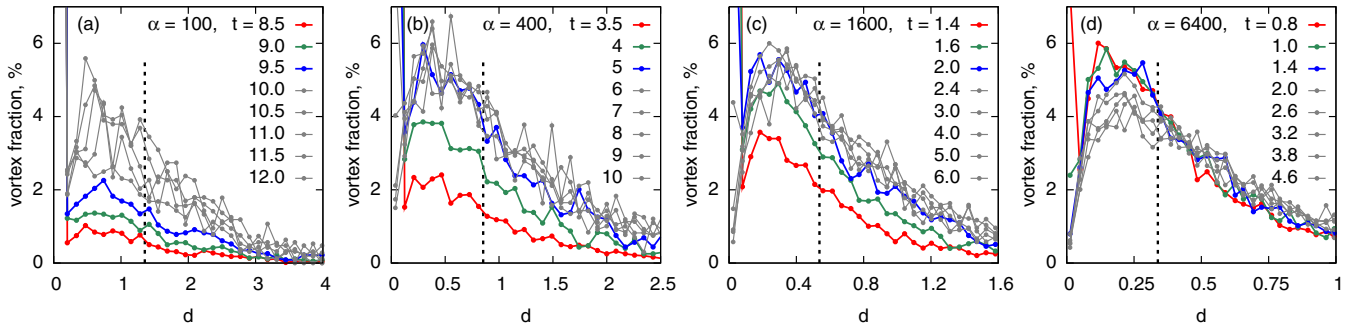

FIG. 11. Histogram of lengths of vortex pairs, obtained in simulations with $L = 32\pi$. The plots show the fraction of vortex pairs in a bin $(d, d + \Delta d)$ of size $\Delta d = 0.1 d_2$, where $d_2 = 2\pi\alpha^{-1/3}$. The scale d_2 is shown with dashed vertical lines.

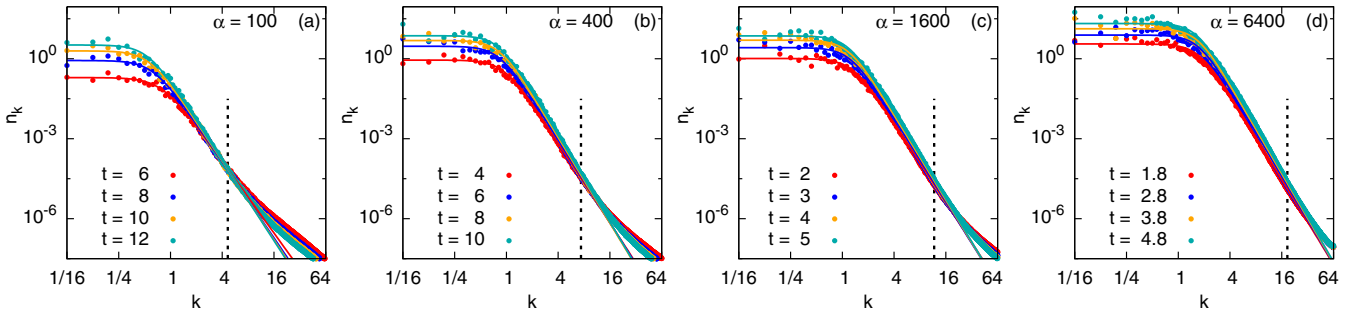

FIG. 12. Spectra at late times for $L = 32\pi$ fitted by Eq. (4). The vertical lines correspond to scale $\lambda_2 = 2\pi/k_2$ with $k_2 = \alpha^{1/3}$.

with the number of vortices dropping from 20 000 to 3000, in the 2π box, while here the number of pairs drops to 2000 in the 32π box.

It is interesting that the straightforward averaging of intervortex distances gives $d_2 \propto d_1 \propto t^{1/5}$. The contradiction with visual observation of constant d_2 is the effects of ultrashort and extra-long dipoles. During the stage of vortex formation, vortices are hard to distinguish from noise; the diagnostics detects a colossal number of vortex pairs with lengths at the limit of resolution. At later times, isolated vortices are formally assigned into pairs as a side effect of our vortex matching algorithm. The number of such pairs is small, but their large lengths significantly affect the average. We found the histograms of the intervortex lengths, shown in Fig. 11, more informative than the average.

In Fig. 11, the system with weakest pumping $\alpha = 100$ is still going through the vortex formation stage, as indicated by the peak at the first bin of the distribution. In the case of $\alpha = 6400$, the fraction in the first bin is insignificant for $t > 1$ and the distribution preserves its shape over the course of the system evolution. In all cases, the number of vortices dropped from $n_{\rm vort} \sim 10\,000$ to $n_{\rm vort} \sim 1000$ during the time interval considered. In all cases, the length $d_2 = 2\pi\alpha^{-1/3}$ is proportional to the distance at the peak of distribution, with a factor $\sim$2.5.

Our observation that the length of a vortex pair depends on the pumping rate, rather than time, is surprising. One would expect the intervortex distance to be proportional to a typical size of the vortex core, which scales as $1/|\psi| \sim N^{-1/2}$ [14]. Such a reduction of intervortex distance was observed in experiments [15] and simulations [16] for vortex pairs moving from regions of less dense condensate to more dense condensate. In contrast, in images shown in Fig. 5, the wave action for the system with $\alpha = 6400$ increases by the factor of 47, which would translate to the decrease of intervortex distances by factor of 7, yet we observe that the intervortex distance is unchanged.

As discussed in the main part of the paper, the length of the vortex pair, d_2, corresponds to the bending point in the spectra, k_2, shown by dashed lined in Fig. 12. Nowak *at al.* [10] made a similar connection between vortices and the shape of the spectra in simulations on thermalization of Gross-Pitaevskii turbulence. First, they inspected the spectrum of a manufactured field of vortices and concluded that (i) the spectrum has a k^{-2} slope on scales greater than the length of a typical vortex pair, (ii) the slope steepens to k^{-4} for scales between the vortex pair and vortex core, and (iii) the slope is k^{-6} on scales below the size of the vortex core. Next they confirmed the presence of k^{-2} and k^{-4} slopes in dynamical simulations (although to observe k^{-2} the authors had to select simulations with the shortest dipoles). As for the k^{-6} slope, the interval of smallest scales was dominated by the spectrum of over-condensate fluctuations, k^{-2}. Forced evolution has different dynamics than thermalization. Even though both types of spectra show qualitatively similar shapes with three distinct exponents, the values of the exponents are different. We observe a plateau (rather than the k^{-2} slope) at largest scales and a midrange slope that gradually increases with time.

APPENDIX D: TRANSITION FROM PRECONDENSATE TO CONDENSATE

We expect the transition from precondensate to condensate to occur when the typical distance between vortex pairs d_1 exceeds the domain size. We consider three domain sizes $L = \pi/2$, π, and 2π and two pumping rates $\alpha = 100$ and 1600 and we estimate the times of the transition to condensate $t_{\rm cond}$ as the abscissa of $d_1 = L$ in Fig. 6. These times are listed in Table I. Among the combinations considered, the transition to condensate in cases (a), (b), and (d) is expected to happen on the border between the stages of vortex formation and vortex annihilation, $t_{\rm cond} \sim 2t^*$; for the other three combinations the transition is expected in the vortex annihilation regime $t_{\rm cond} \gg 2t^*$. For each case, we have performed ten simulation with different random seeds. For each realization, we measured the number of vortex pairs in the domain as a function of time.

First, let us compare simulations with two different pumping rates in the domain of size $L = \pi/2$, cases (a) and

TABLE I. Parameters of simulations in small boxes and time of transition from precondensate to condensate estimated from Fig. 6. Here the data beyond the interpolation range are shown as blank entries.

Case	α	$2t^*$	L	$L\alpha^{1/3}$	$\alpha^{-2/3}t_{\rm cond}$	$t_{\rm cond}$
(a)	100	8.4	$\pi/2$	7.29	194	9
(b)	100	8.4	π	14.58	240	11
(c)	100	8.4	2π	29.16	1500	70
(d)	1600	1.3	$\pi/2$	18.37	220	1.6
(e)	1600	1.3	π	36.74		$t_{\rm cond} \gg 2t^*$
(f)	1600	1.3	2π	73.49		$t_{\rm cond} \gg 2t^*$

(d). In case (a) the last vortices have disappeared during the time range [8.0,10.8], in agreement with the expected $t_{\rm cond} = 9$. In case (d) $t_{\rm cond} = 1.6$, and by the time $t = 2.6$ six out of ten realizations are vortex-free. The other four realizations have a single vortex pair; they become vortex-free by the time $t = 16.6$. This is consistent with the overall dynamics in large boxes: At $\alpha = 100$ the transition between thermal equilibrium and the precondensate regime occurs relatively late, at $t^* \approx 4.2$, vortices become detectable at $2t^* \approx 8.4$, and the slow vortex annihilation regime is not reached until $3t^* \approx 12.6$. On the other hand, for $\alpha = 1600$, $2t^* \approx 1.3$, which explains the disappearance of most of the vortices by time $t = 2.6$. Vortex annihilation becomes slow after $3t^* \approx 2$, which is why it takes so long time (up to $t = 16.6$) for the four remaining pairs to disappear. Simulations with $L = \pi$ and 2π show qualitatively the same results, except that only the

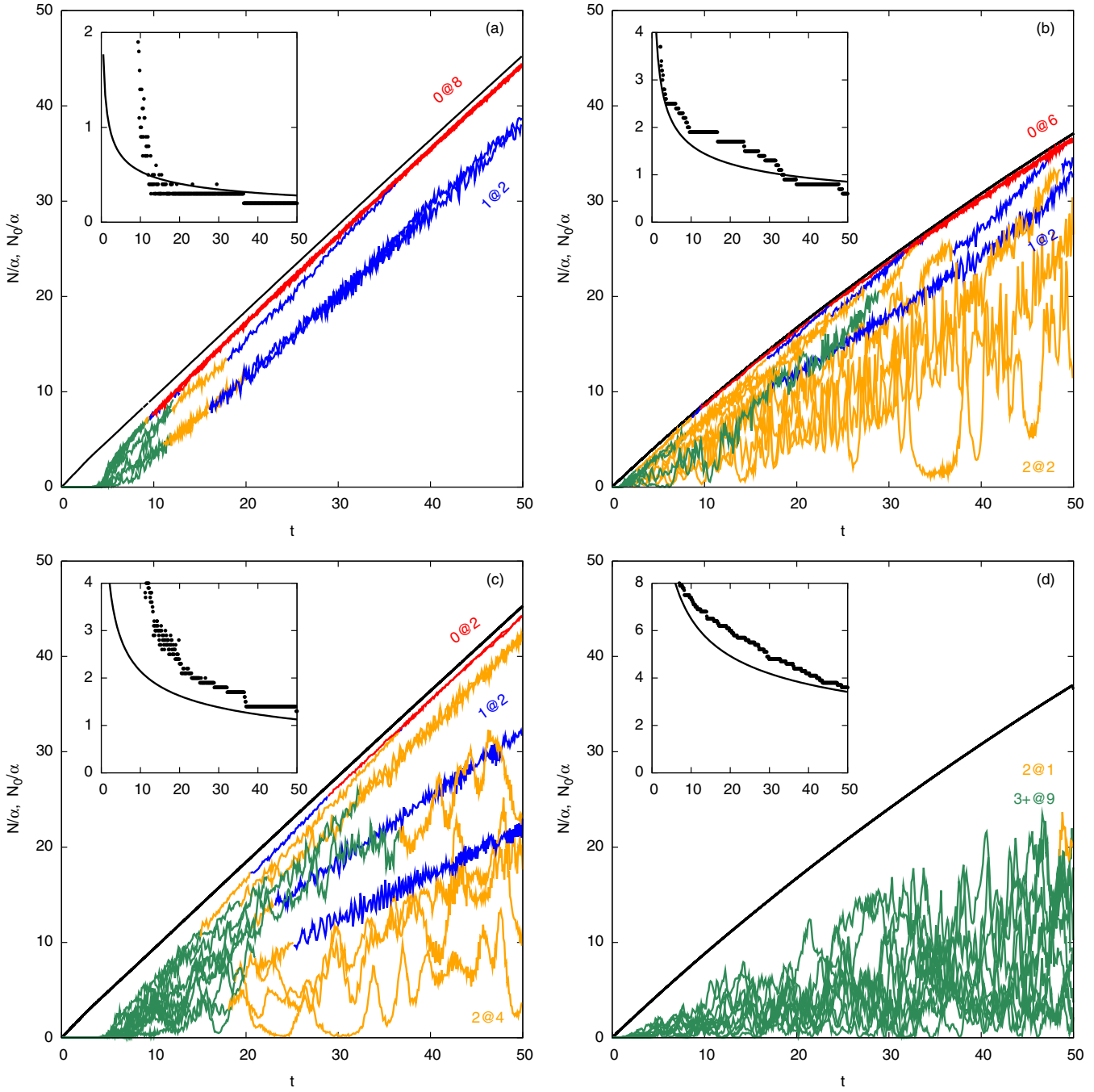

FIG. 13. Establishment of condensate in small domains (a) and (b) $L = \pi$ and (c) and (d) $L = 2\pi$ for (a) and (c) $\alpha = 100$ and (b) and (d) $\alpha = 1600$, ten realizations per case. Black lines show the total number of waves $N(t)$, while colored lines show the number of waves in the condensate $N_0(t)$. The number of vortex pairs averaged among realizations is shown in the insets as a function of time, next to the extrapolation obtained from simulations in large domains (C1). The color of the $N_0(t)$ curves corresponds to the number of vortex pairs in the system: 0 (red), 1 (blue), 2 (yellow), and 3 or more (green). The labels show the state of each ensemble at $t = 50$ in the format $n_{\rm pairs}@n_{\rm realizations}$.

runs from case (b) have good chances of forming systemwide condensates before vortex annihilation becomes slow.

For cases (b), (c), (e), and (f) we compare the wave action $N_0(t)$ accumulated in the condensate (that is, in the $k = 0$ mode) to the wave action of the whole system $N(t)$. The comparison is shown in Fig. 13. Within each set of realizations, the curve $N(t)$ does not depend on realization. (The curves for $\alpha = 1600$ deviate from linear growth because of higher losses to damping at large N.) In contrast, the wave action in the condensate is different in each realization, at least during the time when vortices are still present in the system. When vortices are gone, the wave action of over-condensate fluctuations $N - N_0$ stays at an approximately constant level, with the exceptions of small-amplitude oscillations [17]. Notice that the small level of over-condensate fluctuations $N - N_0 \ll N$ does not guarantee a vortex-free system. Moreover, the systems with the same number of vortices can have different fractions of waves in the condensate and $N - N_0$ is nonmonotonic function of the number of vortex pairs.

The insets in Fig. 13 provide another way to compare the dynamics of vortex annihilation in small and large domains. Here the dots show the number of vortex pairs in small domains, averaged over ten realization, as a function of time. The lines are predictions derived from the extrapolation (C1) for large domains. Qualitatively, the number of vortex pairs in small systems agrees with the dynamics of evolution of large systems.

APPENDIX E: TIME SCALE OF TRANSITION IN PHYSICAL UNITS

The time scale t^* is an important characteristic of the system. Our simulations, done in nondimensional variables, show that $\tilde{t}^* \approx 90(d\tilde{N}/d\tilde{t})^{-2/3}$. (In this appendix we denote nondimensionalized quantities by tildes.) Let us estimate t^* for a physical system.

We restore physical dimensions in Eq. (1),

$$iq^2\tau\psi_t + q^2\ell^2\nabla^2\psi \pm q^2\frac{|\psi|^2}{I_0}\psi = 0,$$

introducing coefficients τ, ℓ, and I_0 that have units of time, length, and wave intensity, respectively. The multiplier q is an arbitrary quantity that parametrizes the family of transformations between simulation units and physical units,

$$t = q^2\tau\tilde{t}, \quad x = q\ell\tilde{x}, \quad \psi = \frac{\sqrt{I_0}}{q}\tilde{\psi}.$$

It is natural to assume that the physical pumping scale ℓ_p is known. Then we can use it to select the transformation parameter $q = \ell_p/\ell\tilde{\ell}_p$, where $\tilde{\ell}_p = 2\pi/80$ is the pumping scale in our simulation units. Thus, we obtain

$$t^* \approx 16.5\tau\left[\frac{\ell_p}{\ell}\frac{\tau}{I_0}\dot{N}\right]^{-2/3},$$

where $N = \langle|\psi|^2\rangle$.

[1] V. E. Zakharov, V. S. Lvov, and G. Falkovich, *Kolmogorov Spectra of Turbulence I: Wave Turbulence* (Springer, New York, 1992).

[2] G. Falkovich and A. Shafarenko, J. Nonlinear Sci. **1**, 457 (1991).

[3] C. Connaughton, A. C. Newell, and Y. Pomeau, Physica D **184**, 64 (2003).

[4] L. P. Pitaevskii and S. Stringari, *Bose-Einstein Condensation* (Clarendon, Oxford, 2003).

[5] S. Dyachenko, A. C. Newell, A. Pushkarev, and V. E. Zakharov, Physica D **57**, 96 (1992).

[6] S. Nazarenko and M. Onorato, Physica D **219**, 1 (2006).

[7] C. Sulem and P. L. Sulem, *Nonlinear Schrödinger Equations: Self-Focusing and Wave Collapse* (World Scientific, New York, 1999).

[8] N. Bogoliubov, J. Phys. (USSR) **11**, 23 (1947).

[9] A. Dyachenko and G. Falkovich, Phys. Rev. E **54**, 5095 (1996).

[10] B. Nowak, J. Schole, D. Sexty, and T. Gasenzer, Phys. Rev. A **85**, 043627 (2012).

[11] J. Schole, B. Nowak, and T. Gasenzer, Phys. Rev. A **86**, 013624 (2012).

[12] G. Falkovich and N. Vladimirova, Phys. Rev. E **91**, 041201 (2015).

[13] N. Vladimirova, S. Derevyanko, and G. Falkovich, Phys. Rev. E **85**, 010101 (2012).

[14] L. P. Pitaevskii, Sov. Phys. JETP **13**, 451 (1961).

[15] T. W. Neely, E. C. Samson, A. S. Bradley, M. J. Davis, and B. P. Anderson, Phys. Rev. Lett. **104**, 160401 (2010).

[16] L. A. Smirnov and V. A. Mironov, Phys. Rev. A **85**, 053620 (2012).

[17] P. Miller, N. Vladimirova, and G. Falkovich, Phys. Rev. E **87**, 065202 (2013).